Passive Filter Design Algorithm for Transient Stabilization of Automotive Power Systems

Martin Baumann[13], Ali Shoar Abouzari[13], Christoph Weissinger[1], Bjørn Gustavsen[2], Hans-Georg Herzog[3]
[1]BMW Group, Germany; [2]SINTEF Energy Research, Norway; [3]Technical University of Munich, Germany
mr.baumann@tum.de, a.shoar@tum.de

***Abstract*—The automotive power system is being increasingly expanded by adding high-dynamic power electronics. These components can potentially cause malfunction or failure of safety-relevant low-voltage components. The susceptibility to disturbances is often reduced by usage of oversized passive input electronics. This paper introduces an alternative means of disturbance suppression by the introduction of system integrated adaptive passive filters. A proposed methodology is presented for examining the suitability of potential access points within complex networks. An algorithmic procedure for the parametrization of several switchable bandpass filter stages is explained. The in-vehicle measurement demonstrates the effectiveness of the dimensioned filter being able to reduce disturbances at 70 kHz by more than 75 %.**

I. Motivation and Related Work

Especially the integration of crucial automated driving functions highlights the importance of the safety-critical automotive power systems. At the same time, power electronics lead to high-dynamic load fluctuations. Potential triggered disturbances can cause malfunctions of safety-relevant components. Their function is required for the safe operation of the vehicle and therefore they must be reliably supplied.

Previous publications limit their focus on the power system stabilization below 10 kHz. Necessary measures have been identified as low-ohmic harness architectures, the integration of supercapacitors, the temporal shift of peak power consumptions and power degradation or shut down of stability critical consumers. [1]–[4]

Power fluctuations and voltage oscillations with prominent frequencies above 10 kHz can negatively influence the safe operation of components. Transient voltage suppressors and Zener diodes are used to suppress voltage transients as shown in [5]. Transients with time constants as low as 20 µs are specified in ISO7637 [6]. Electrical filters can be used to stabilize the dynamic behavior of the power systems as demonstrated in [7]. Current pulses replicate dynamic loads [8].

Passive filters for suppression of harmonics have been deeply investigated for high-voltage AC transmission and distribution grids. Commonly used topologies are highpass, C-type, shunt and bandpass filters. [9], [10]

Passive bandpass filters were applied to automotive high-voltage power systems. Voltage oscillations due to power electronic devices can be suppressed as verified in [11].

However, there are fundamental structural differences between high and low-voltage power systems such as harness geometry and number of components. This contribution aims to create a decentralized approach to reduce system-inherent disturbances within low-voltage power systems. Electrical requirements to attached components can be scaled down.

The specific contributions in this paper are:

- Methodology to quickly and accurately identify system-inherent disturbances in the range of 10 kHz to 100 kHz.
- Algorithmic determination of adaptive multi-stage filter location and parametrization.
- Validation by means of a future generation highly automated vehicle based test bench demonstrates the effectivity of passive filters regarding transient stabilization.

II. Transient Vehicular Disturbances

The filter calculation requires an in-depth knowledge of the automotive power system. Therefore, this chapter summarizes the specific motivation by means of a customized example.

Fig. 2 shows a feasible tree structure vehicular low-voltage power system. The system is supplied by a DC/DC converter ensuring the bidirectional power flow to the high-voltage system. Two current distributors CD1, CD2 are attached through harness impedances $Z_{\mathrm{h,cd}}$. Both distributors include safety-relevant components in accordance to Automotive Safety-Integrity Level (ASIL) and Quality Consumers (QM).

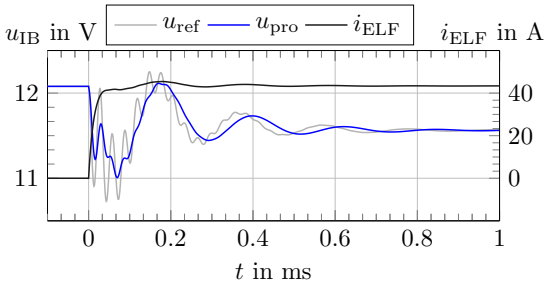

(a) QM load step with current slope of 1 MA/s.

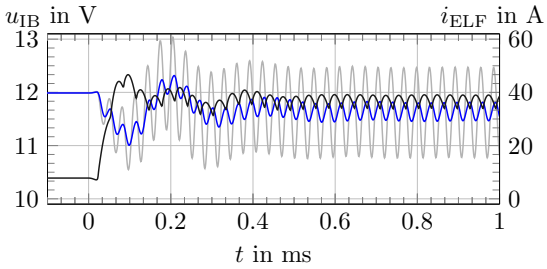

(b) QM load oscillation of 5 A at 30 kHz.

Fig. 1: High dynamic power fluctuations contrasting QM current profiles i_{ELF} and ASIL voltages u_{IB} without filter u_{ref} and with proposed filter u_{pro}.

This is the accepted version of a paper presented at 2021 IEEE 93rd Vehicular Technology Conference - VTC2021-Spring : Proceedings
http://dx.doi.org/10.1109/VTC2021-Spring51267.2021.9449066

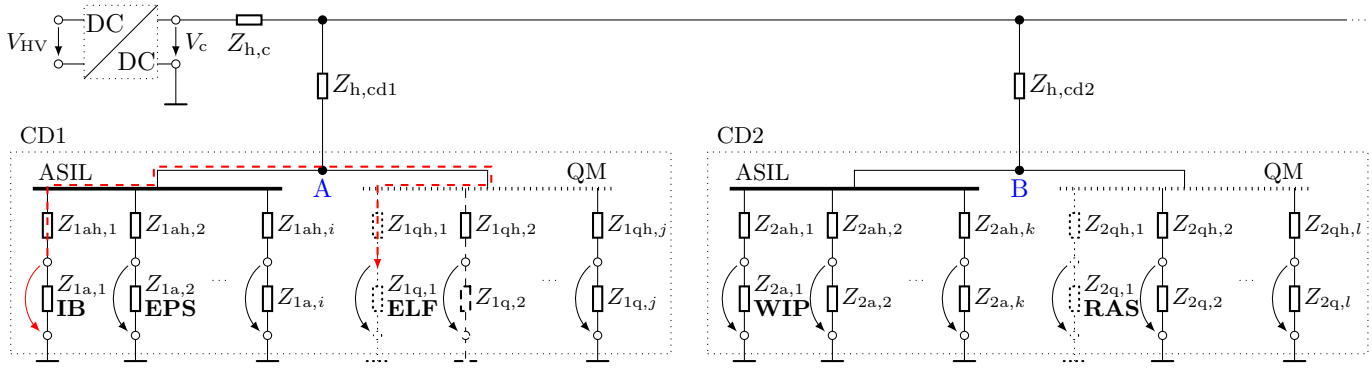

Fig. 2: Tree structure based automotive low-voltage power system consists of a DC/DC converter, several harness impedances Z_h and current distributors CD1, CD2 with ASIL and QM consumers such as Integrated Brake (IB), Electric Power Steering (EPS), Wipers (WIP), Electric Fan (ELF) and Rear Axle Steering (RAS).

Safety relevant components such as Integrated Brake (IB), Electric Power Steering (EPS) and Wipers (WIP) belong to the group of ASIL. Comfort consumers such as Electric Fan (ELF) and driving dynamics refinements such as Rear Axle Steering (RAS) belong to QM.

CD1 includes i ASIL components $Z_{1a,i}$ being attached to its access point A through harness impedances $Z_{1ah,i}$. The same analogy applies for j QM components of CD1, k ASIL and l QM components of CD2. Fig. 2 can be expanded by several current distributors to map the entire vehicular power system.

Disturbances of interest occur for QM components drawing fluctuating power from the system. Voltages at the terminals of neighboring components are particulary disturbed. Fig. 2 redly highlights the exemplary disturbance path $i_{ELF} \rightarrow u_{IB}$ of IB $Z_{1a,1}$ as a consequence of load fluctuations of ELF $Z_{1q,1}$.

Fig. 1 contrasts load fluctuations of QM component ELF and the voltage at terminals of ASIL component IB. The simulation was carried out on the exemplary simplified power system of Fig. 2 for the redly highlighted power transfer path.

A 500 W load jump at the current slope of 1 MA/s is examined in Fig. 1a. Voltage u_{IB} strongly oscillates without any taken measures as displayed in grey. The voltage lowers to 10.6 V. By integrating the proposed filter being described in Section IV, the bluely highlighted voltage drop can be reduced by 30 % to a minimum of 11 V.

Fig. 1b demonstrates the simulated system reaction to an oscillating load at 30 kHz of 13 % or 5 A, respectively. Under steady state condition at 0.5 ms the unfiltered voltage oscillates about 1.7 V, where the filter leads to an oscillation of 0.4 V. The integrated filter effectively reduces the voltage disturbance by more than 76 %.

III. Modeling

Disturbances as shown in Fig. 1 arise due to anti-resonances in the transfer impedance. These anti-resonances are caused by the series structure of cable inductance and component integrated input circuitries capacitances. An anti-resonance provides a comparably low-impedance path for the transient current. This creates an excessive voltage disturbance at the terminals of the susceptible component. Fig. 3 shows a bluely highlighted exemplary transfer impedance. The graph clearly visualizes a pronounced anti-resonance of 1 Ω at 30 kHz.

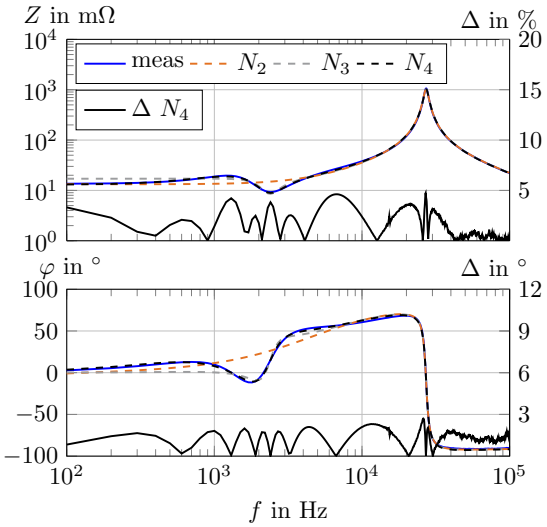

Fig. 3: Approximation of an exemplary transfer impedance using vector fitting. Appoximating with $N = 4$ leads to a satisfying accuracy with a deviation Δ of less than 5 %.

A. System Identification

In order to replicate this measurement in a transient simulation environment, it needs real passive impedance based modeling. The active control and non-linearities as well as the electromechanical load of actuators can be neglected [12]. The basis is the impedance spectra being determined by network analyzers measurement. The resulting impedance spectra need to be transformed into passive RLC-based networks by means of network synthesis such as Bott-Duffin synthesis being described in detail in [12]–[14].

The goal of the accurate modeling is the systematic manipulation of unfavorable spectra. Therefore, the spectra are described in the mathematical s-domain. A computationally efficient method for system identification is vector fitting [15], [16]. Vector fitting is a methodology for the approximation of rational functions in frequency domain on the basis of measured or computed frequency responses.

This is the accepted version of a paper presented at 2021 IEEE 93rd Vehicular Technology Conference - VTC2021-Spring : Proceedings
http://dx.doi.org/10.1109/VTC2021-Spring51267.2021.9449066

The methodology generates a structure as shown in (1). The number of partial fractions N can be of any size in dependence of target accuracy and complexity of underlying data. Residues c_n and poles a_n are either real or complex conjugated pairs. Additionally, a gain d or inductive behavior h could exist. The calculation of transfer function (1) is nonlinear since both coefficients of numerator and denominator are unknown. Vector fitting iteratively relocates an initial set of poles to better positions while solving a linear least-squares problem.

$$F(s) \approx \sum_{n=1}^{N} \frac{c_n}{s - a_n} + d + h \cdot s \tag{1}$$

Fig. 3 shows the resulting approximations of the applied vector fitting algorithm for the exemplary transfer impedance in the frequency range 0.1 kHz to 100 kHz. The bluely highlighted measured original spectrum is contrasted to three orders of approximation $\{2, 3, 4\} \in N$. $N = 4$ sufficiently replicates the original with a maximum deviation of 5 % in amplitude and 3° in phase. Further approximations $N = 2$, $N = 3$ result in deviations of 61 % and 26 %, respectively. For the application of filter computation, resonances and anti-resonances need to be represented sufficiently. The complexity of resulting transfer functions is reduced through neglecting poles and zeros above the frequency range of interest. Furthermore, pole-residue terms with small c_n/a_n ratios are excluded since they do not contribute to the model behavior.

B. Two-Port Abstraction

Disturbances occur due to the electrical connection between source and receiver. Fig. 4 illustrates the assumptions the filter calculation is based on. Disturbance source Z_s can be a consumer or an energy source such as a DC/DC converter being capable to enforce high dynamic power fluctuations. Disturbance receiver Z_r is a highly susceptible and safety-relevant consumer such as IB, EPS, WIP, sensors or computation devices. Filter Z_f is connected to the electrical path in order to reduce disturbances. Source, receiver and filter are attached to different access points of the grid: $\mathrm{AP_s}$, $\mathrm{AP_r}$, $\mathrm{AP_f}$.

The remaining grid is summarized in a simplified manner. Connection characteristics are integrated in star topology as two-ports $\mathrm{TP_s}$, $\mathrm{TP_r}$, $\mathrm{TP_f}$ intersecting in Node O. The present illustration can be used in any configuration of a tree structure based power system.

$$\boldsymbol{H} = \begin{bmatrix} H_{11} = \left.\frac{U_1}{I_1}\right|_{U_2=0} & H_{12} = \left.\frac{U_1}{U_2}\right|_{I_1=0} \\ H_{21} = \left.\frac{I_2}{I_1}\right|_{U_2=0} & H_{22} = \left.\frac{I_2}{U_2}\right|_{I_1=0} \end{bmatrix} \tag{2}$$

The representation of two-ports by means of hybrid matrices is particularly advantageous as illustrated in (2). H-parameters H_{11}, H_{12}, H_{21} and H_{22} are calculated by means of shown impedances Z_g, Z_1 and Z_2 according to (3) and Fig. 4.

$$\begin{aligned} H_{11} &= Z_1 + Z_\mathrm{g} || Z_2 & H_{22} &= -\frac{1}{Z_\mathrm{g} + Z_2} \\ H_{12} &= H_{21} = \frac{Z_\mathrm{g}}{Z_\mathrm{g} + Z_2} \end{aligned} \tag{3}$$

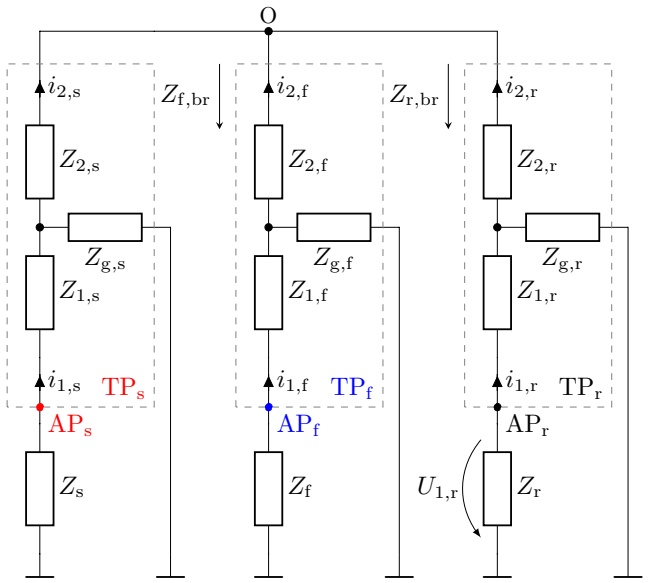

Fig. 4: Simplified two-port based abstraction of the power system with disturbance source Z_s, disturbed receiver Z_r and suppression filter Z_f.

Each H-parameter is an s-domain function and is part of the two-port representations for source $\boldsymbol{H_\mathrm{s}}$, receiver $\boldsymbol{H_\mathrm{r}}$ and filter $\boldsymbol{H_\mathrm{f}}$. The transfer impedance from source to receiver $Z_{\mathrm{s}\to\mathrm{r}}$ is calculated according to (4). The equation results from two-port expressions (2), (3) on the basis of newly introduced auxiliary functions M_r, M_1, M_2, M_3 and M_4 as shown in (5).

$$Z_{\mathrm{s}\to\mathrm{r}} = \frac{U_{1,\mathrm{r}}}{I_{1,\mathrm{s}}} = \frac{M_1 \cdot Z_\mathrm{f} + M_2}{M_3 \cdot Z_\mathrm{f} + M_4} \tag{4}$$

$$\begin{aligned} M_\mathrm{r} &= \frac{1}{H_{12,\mathrm{r}} - H_{22,\mathrm{r}} \cdot \frac{Z_\mathrm{r} + H_{11,\mathrm{r}}}{H_{12,\mathrm{r}}}} \\ M_1 &= Z_\mathrm{r} \cdot M_\mathrm{r} \cdot H_{21,\mathrm{s}} \\ M_2 &= Z_\mathrm{r} \cdot M_\mathrm{r} \cdot H_{21,\mathrm{s}} \cdot H_{11,\mathrm{f}} \\ M_3 &= 1 - (H_{22,\mathrm{s}} + H_{22,\mathrm{f}}) \cdot Z_{\mathrm{r,br}} \\ M_4 &= (1 - H_{22,\mathrm{s}} \cdot Z_{\mathrm{r,br}}) \cdot H_{11,\mathrm{f}} \\ &\quad + Z_{\mathrm{r,br}} \cdot \left(H_{12,\mathrm{f}}^2 - H_{11,\mathrm{f}} \cdot H_{22,\mathrm{f}}\right) \end{aligned} \tag{5}$$

The introduced two-port abstraction describes any interference path within the automotive power system between two points in dependence of filter impedance Z_f at any chosen filter location. A transfer impedance $Z_{\mathrm{s}\to\mathrm{r}}^{\mathrm{wof}}$ without filter can be calculated for reference purposes. The equation shows the derivation from an open loop filter impedance in (6). Noticeably, this transfer impedance is independent from source impedance Z_s. Moreover, the return path can be calculated in a similar way. This will be applied to ensure bidirectional disturbance suppression.

$$Z_{\mathrm{s}\to\mathrm{r}}^{\mathrm{wof}} = \lim_{Z_\mathrm{f}\to\infty} Z_{\mathrm{s}\to\mathrm{r}} = \frac{M_1}{M_3} \tag{6}$$

This is the accepted version of a paper presented at 2021 IEEE 93rd Vehicular Technology Conference - VTC2021-Spring : Proceedings
http://dx.doi.org/10.1109/VTC2021-Spring51267.2021.9449066

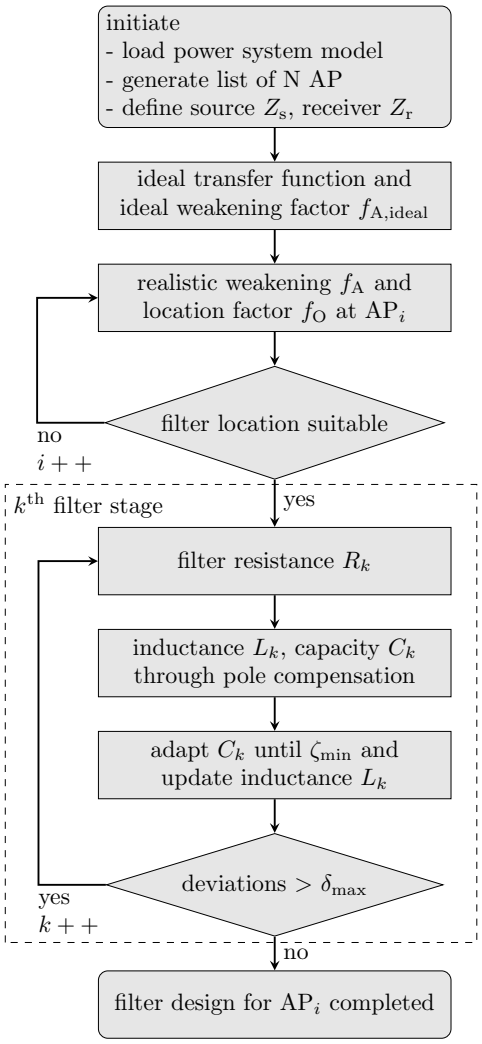

Fig. 5: Flowchart of the filter design algorithm.

TABLE I: Symbols and Abbreviations.

AP	Access Point
Z_s, Z_r, Z_f	Source, Receiver and Filter Impedances
f_A	Weakening Factor
f_O	Location Factor
R_k, C_k, L_k	Resistance, Capacitance, Inductance of k^{th} Filter Stage
ζ_{min}	Minimum Effectiveness of C_k
δ_{max}	Maximum Deviation from Original Transfer Function

IV. Algorithmic Filter Design

Fig. 5 shows the algorithmic filter design. After loading of the power system model, generation of N potential access points (AP_f) and definition of disturbance path, the ideal transfer function is calculated. Weakening f_A and location factors f_O at the anti-resonance frequency f_0 for a chosen suitable AP$_i$ are specified. Once found an appropriate location, filter parameters R_k, L_k, C_k of the k^{th} filter stage are calculated. If positive deviations occur from the target, further filter stages $k > 1$ are calculated. The process can be repeated for other APs and the same transfer function.

A. Ideal Target Transfer Function

The application of a passive filter to the power system aims to weaken anti-resonances that are caused by a complex conjugated critical pole pair p_l, p_l^* of a given transfer function. By means of these poles, oscillation frequencies ω_0 or f_0 and damping factor D_0 are calculated according to (7).

$$\begin{aligned} s^2 - (p_l + p_l^*)\, s + p_l \cdot p_l^* &= s^2 - 2 \cdot \mathfrak{Re}\,(p_l)\, s + \omega_0^2 \\ &= s^2 + 2D_0\omega_0 s + \omega_0^2 \end{aligned} \tag{7}$$

A pronounced anti-resonance occurs for low real parts $\mathfrak{Re}\,(p_l)$ or high imaginary parts. The idea is to weaken the anti-resonance through elevating the real part of the oscillation causing poles. Fig. 6 highlights poles and zeros of the exemplary transfer impedance $i_{ELF} \rightarrow u_{IB}$. The transfer impedance is visualized in Fig. 7 in grey. Two complex conjugated poles p_l with big imaginary part cause the anti-resonance at 32.1 kHz. An elevation of the real part while keeping the absolute value $p_{l,ideal}$ results in the new damping factor D_{new}. The anti-resonance is weakened while its frequency remains. Weakening factor f_A is introduced in (8). This ratio also expresses the value by which the amplitude of the anti-resonance is reduced. The ideal weakening factor $f_{A,ideal}$ is given in (9). Poles are greenly highlighted in Fig. 6. These poles come about for complete damping of the anti-resonance with the ideal damping factor $f_{A,ideal}$.

$$f_A = \frac{D_{new}}{D_0} = \frac{\mathfrak{Re}\,(p_{l,new})}{\mathfrak{Re}\,(p_l)} \tag{8}$$

$$f_{A,ideal} = \frac{\mathfrak{Re}\,(p_{l,ideal})}{\mathfrak{Re}\,(p_l)} = \sqrt{1 + \frac{\mathfrak{Im}\,(p_l)^2}{\mathfrak{Re}\,(p_l)^2}} \tag{9}$$

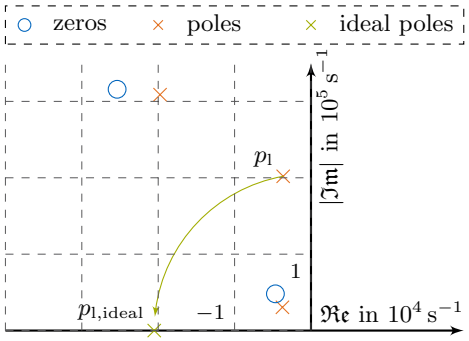

Fig. 6: Pole-zero map of transfer impedance ELF to IB ($i_{ELF} \rightarrow u_{IB}$). Critical poles are circular shifted to the real axis while keeping their absolute value. The difference of axis scaling is neglected to point out the circular shift of poles.

The ideal damped transfer function is indicated in Fig. 7 in dashed blue and contrasted to the original in grey.

B. Passivity

The resulting theoretically calculated filter impedance on the basis of the ideal damped anti-resonance and the ideal target transfer function is not necessarily passive. Fig. 7 shows the ideal filter impedance in dashed green. An impedance is only

This is the accepted version of a paper presented at 2021 IEEE 93rd Vehicular Technology Conference - VTC2021-Spring : Proceedings
http://dx.doi.org/10.1109/VTC2021-Spring51267.2021.9449066

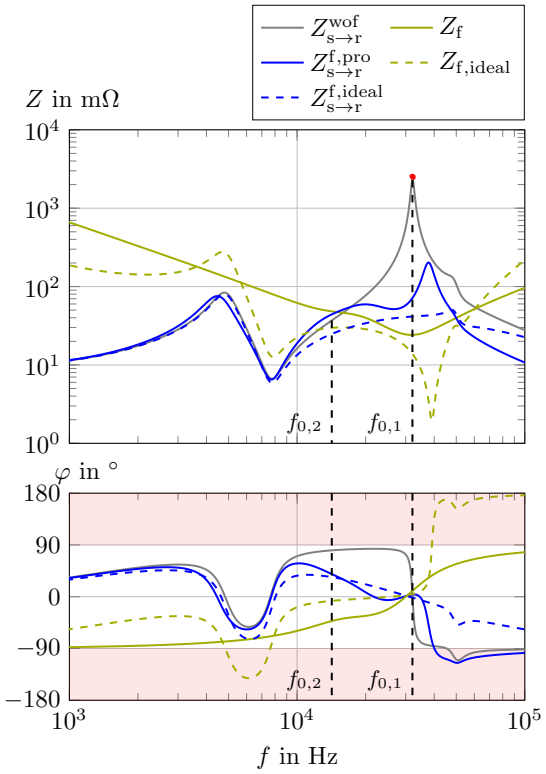

Fig. 7: The calculated two-staged filter (attached to AP A in CD1) changes the original transfer impedance ($Z^{\mathrm{wof}}_{\mathrm{s}\to\mathrm{r}}$) to $Z^{\mathrm{f,pro}}_{\mathrm{s}\to\mathrm{r}}$, while the ideal filter results in $Z^{\mathrm{f,ideal}}_{\mathrm{s}\to\mathrm{r}}$.

feasible in passive fashion when equations (10) are satisfied. The impedances phase needs to be forced to the range of $-90°$ to $90°$. Otherwise, the filter would not be passive but would be able to feed in power. Moreover, Fig. 7 indicates a pure resistive filter behavior at the anti-resonance $f_{0,1}$.

$$\begin{aligned} \Re\mathfrak{e}\left(Z\left(s\right)\right) > 0 \quad &\text{for} \quad \Re\mathfrak{e}\left(s\right) > 0 \\ \Im\mathfrak{m}\left(Z\left(s\right)\right) = 0 \quad &\text{for} \quad \Im\mathfrak{m}\left(s\right) = 0 \end{aligned} \tag{10}$$

C. Implementation with Bandpass Filters

To calculate a filter impedance for an anti-resonance at ω_0, its characteristics are found based on a target transfer impedance in dependence of target damping factor f_{A} deviating from $f_{\mathrm{A,ideal}}$. Assuming an identical phase at ω_0, the ohmic resistance of the filter stage is calculated according to (11) with f_{A}. The values for L and C are determined by introducing the critical pole p compensating zeros z_{n} in (12).

$$R\left(f_{\mathrm{A}}\right) = \Re\mathfrak{e}\left(\frac{f_{\mathrm{A}} \cdot M_2\left(j\omega_0\right) - M_4\left(j\omega_0\right) \cdot Z_{\mathrm{s}\to\mathrm{r}}\left(j\omega_0\right)}{M_3\left(j\omega_0\right) \cdot Z_{\mathrm{s}\to\mathrm{r}}\left(j\omega_0\right) - f_{\mathrm{A}} \cdot M_1\left(j\omega_0\right)}\right) \tag{11}$$

$$z_{\mathrm{n}} \stackrel{!}{=} \Re\mathfrak{e}\left(p\right) + j\Im\mathfrak{m}\left(p\right) = p_{\mathrm{r}} + jp_{\mathrm{i}} \tag{12}$$

The new transfer function equation at the zeros z_{n} needs to be zero for full compensation (13). M_i with $\{1,2,3,4\} \in i$ (5) consists of numerator $M_{i,\mathrm{Z}}$ and denominator $M_{i,\mathrm{N}}$.

$$\begin{aligned} &M_{1,\mathrm{Z}}\left(z_{\mathrm{n}}\right) \cdot M_{2,\mathrm{N}}\left(z_{\mathrm{n}}\right) \cdot Z_{\mathrm{f,Z}}\left(z_{\mathrm{n}}\right) \\ &+M_{2,\mathrm{Z}}\left(z_{\mathrm{n}}\right) \cdot M_{1,\mathrm{N}}\left(z_{\mathrm{n}}\right) \cdot Z_{\mathrm{f,N}}\left(z_{\mathrm{n}}\right) \stackrel{!}{=} 0 \end{aligned} \tag{13}$$

Inductance L and capacitance C of the filter stage that compensate critical poles are calculated according to (14).

$$\begin{aligned} L &= \frac{1}{2\,p_{\mathrm{r}}\,p_{\mathrm{i}}}\left[\Im\mathfrak{m}\left(\frac{-M_{2,\mathrm{Z}}\left(p\right)\,M_{1,\mathrm{N}}\left(p\right)\,p}{M_{1,\mathrm{Z}}\left(p\right)\,M_{2,\mathrm{N}}\left(p\right)}\right) - R\,p_{\mathrm{i}}\right] \\ \frac{1}{C} &= \Re\mathfrak{e}\left(\frac{-M_{2,\mathrm{Z}}\left(p\right)\,M_{1,\mathrm{N}}\left(p\right)\,p}{M_{1,\mathrm{Z}}\left(p\right)\,M_{2,\mathrm{N}}\left(p\right)}\right) - L\left(p_{\mathrm{r}}^2 - p_{\mathrm{i}}^2\right) - R\,p_{\mathrm{r}} \end{aligned} \tag{14}$$

Substituting poles and shifting to the real axis does not necessarily end in real positive parameters for L and C. Compensation of critical poles with zeros is highly susceptible to parameter variations and therefore not practically pursued. Instead, start values for the algorithmic solution are generated according to the pole compensation in (14). Precise values are determined by means of the relation indicated in (15).

$$\omega_0 L - \frac{1}{\omega_0 C} = \Im\mathfrak{m}\left(\frac{f_{\mathrm{A}}\,M_2\left(j\omega_0\right) - M_4\left(j\omega_0\right)\,Z_{\mathrm{s}\to\mathrm{r}}\left(j\omega_0\right)}{M_3\left(j\omega_0\right)\,Z_{\mathrm{s}\to\mathrm{r}}\left(j\omega_0\right) - f_{\mathrm{A}}\,M_1\left(j\omega_0\right)}\right) \tag{15}$$

With only one filter stage, there are positive deviations δ arising from the resulting transfer function to original transfer function. The smaller C the more selective is its behavior in relation to frequency. The deviation δ for lower frequencies can get significant for small C. An elevated capacitance C reduces δ. At a certain value of C an aperiodic approximation to a minimum reachable δ appears. The deviation δ follows a hyperbolic decline in contrast to increasing capacitances C.

For an algorithmic calculation, a definition of a limit criterion is suitable. First C is defined within given limitations while the effectiveness is above a certain criterion ζ_{min} being defined as reduction of the deviation δ above capacitances C.

D. Practical Restrictions

The filters PCB implementation comes along with resistances through vias and clampings. Moreover, inductances and capacitances comprise resistive parasitics. The filters inductance is increased by vias L_{via}. The inequalities (16) summarize practical restrictions with average resistances of L, C named as $R_{\mathrm{L,C}}$ and component parameters R_{C}, L_{C}, C_{C}.

$$\begin{aligned} R_{\mathrm{L,C}} + R_{\mathrm{via}} + R_{\mathrm{C,min}} \stackrel{!}{<} R \stackrel{!}{<} R_{\mathrm{L,C}} + R_{\mathrm{via}} + R_{\mathrm{C,max}} \\ L_{\mathrm{via}} + L_{\mathrm{C,min}} \stackrel{!}{<} L \stackrel{!}{<} L_{\mathrm{via}} + L_{\mathrm{C,max}} \\ C_{\mathrm{C,min}} \stackrel{!}{<} C \stackrel{!}{<} C_{\mathrm{C,max}} \end{aligned} \tag{16}$$

E. Further Filter Stages

The mentioned positive deviation from original transfer function δ can be effectively reduced by means of further filter stages. While the first filter stage tries to get the weakening factor f_{A} as close as possible to ideal one, further stages k only compensate positive deviations according to (17).

$$f_{\mathrm{A},k} = \frac{\left|Z_{\mathrm{s}\to\mathrm{r}}\left(j\omega_{0,k}\right)\right|}{\left|Z^{\mathrm{wof}}_{\mathrm{s}\to\mathrm{r}}\left(j\omega_{0,k}\right)\right|} \tag{17}$$

The amplitude of the transfer impedance without filter resistance R_k at the frequency location of the maximum positive

This is the accepted version of a paper presented at 2021 IEEE 93rd Vehicular Technology Conference - VTC2021-Spring : Proceedings
http://dx.doi.org/10.1109/VTC2021-Spring51267.2021.9449066

deviation $\omega_{0,k}$ is introduced as $\left|Z^{\mathrm{wof}}_{\mathrm{s}\to\mathrm{r}}\left(j\omega_{0,k}\right)\right|$. The resistance of the new filter stage R_k is calculated according to (18). Auxiliary functions $M_{1,k}$, $M_{2,k}$, $M_{3,k}$, $M_{4,k}$ are updated with consideration of prior defined filter stages (at least first filter stage was defined before).

$$R_k = \Re\mathfrak{e}\left(\frac{f_{\mathrm{A},k}\, M_{2,k}\left(j\omega_{0,k}\right) - M_{4,k}\left(j\omega_{0,k}\right)\, Z_{\mathrm{q}\to\mathrm{s}}\left(j\omega_{0,k}\right)}{M_{3,k}\left(j\omega_{0,k}\right)\, Z_{\mathrm{q}\to\mathrm{s}}\left(j\omega_{0,k}\right) - f_{\mathrm{A},k}\, M_{1,k}\left(j\omega_{0,k}\right)}\right) \tag{18}$$

The calculation of L_k, C_k follows the procedure as introduced for the first filter stage and visualized in flowchart 5.

F. Abortion of Adding Filter Stages

When a maximum deviation of $\delta_{\max}$ of the resulting transfer impedance from the target impedance is not exceeded within the entire frequency range of interest, the process is ended.

TABLE II: Parameters for exemplary filter design of path ELF to IB ($i_{\mathrm{ELF}} \to u_{\mathrm{IB}}$).

Parameter	Value	Parameter	Value	Parameter	Value
$\delta_{\max}$	10 mΩ	$\zeta_{\min}$	1 %/µF	$R_{\mathrm{L,C}}$	20 mΩ
R_{via}	5 mΩ	$R_{\mathrm{C,min}}$	1 mΩ	$R_{\mathrm{C,max}}$	1000 Ω
L_{via}	10 nH	$L_{\mathrm{C,min}}$	50 nH	$L_{\mathrm{C,max}}$	10 µH
$C_{\mathrm{C,min}}$	10 µF	$C_{\mathrm{C,max}}$	1000 µF		

G. Filter Location

For each critical path P and potential filter location l (AP_{f}) a location factor f_{O} according to (19) is to be calculated. The factor depends on the ideal weakening factor $f_{\mathrm{A,ideal}}$ and realizable weakening factor f_{A}.

$$f_{\mathrm{O}}\left(l,p\right) = \frac{f_{\mathrm{A}}}{f_{\mathrm{A,ideal}}} \tag{19}$$

The realizable weakening factor f_{A} is defined in (20) with R being the minimal achievable resistance on the PCB implementation.

$$f_{\mathrm{A}} = \max\left\{\left|Z_{\mathrm{s}\to\mathrm{r}}\left(j\omega_0\right)\right| \frac{\left|M_3\left(j\omega_0\right)R + M_4\left(j\omega_0\right)\right|}{\left|M_1\left(j\omega_0\right)R + M_2\left(j\omega_0\right)\right|}, f_{\mathrm{A,ideal}}\right\}$$
$$R = R_{\mathrm{L,C}} + R_{\mathrm{via}} + R_{\mathrm{C,min}} \tag{20}$$

For the integration of filters as disturbance reduction for multiple paths an overall location factor (21) is introduced for a specific filter location l_j. The sum of all path P_i (with N_{P} paths) dependent location factors f_{O} multiplied with the amplitude of anti-resonances $A(P_i)$ and path priority $r(P_i)$ builds up the overall location factor. The priority is equal to a value between 0 and 1 and is taken from the evaluation of the entire system. A high priority is given for high safety-relevance of interference receiver Z_{r}. Furthermore, the priority is set to a high value when critical frequencies are acoustically perceptible by humans. Also, an elevated frequency of occurance of dynamic power fluctuations by disturbance source Z_{s} positively influences the priority $r(P_i)$.

$$F_{\mathrm{O}}\left(l_j\right) = \sum_{i=1}^{N_{\mathrm{P}}} f_{\mathrm{O}}\left(l_j, P_i\right) \cdot A\left(P_i\right) \cdot r\left(P_i\right) \tag{21}$$

TABLE III: System design parameters for the introduced exemplary power system.

path P	$r\left(P\right)$	$A\left(P\right)$ in mΩ	f_{O} (CD 1)	f_{O} (CD 2)
RAS → EPS	0.50	275.0	0.3803	0.0930
IB → WIP	0.25	5097.0	0.4465	1.0000
ELF → EPS	0.75	743.7	0.4229	0.1208
ELF → IB	1.00	2294.0	0.5653	0.1180
F_{O}			2.154 Ω	1.625 Ω

From Table III, filter location CD1 can be identified as suitable to reduce disturbances of multiple paths. This takes into consideration the amplitudes of the unique transfer impedances as well as the path priorities. A filter at this location would act as a central device reducing critical disturbances in the frequency range of interest 10 kHz to 100 kHz.

Calculated filter parameters for the disturbance reduction on path $i_{\mathrm{ELF}} \to u_{\mathrm{IB}}$ are listed in Table IV. The two-staged filter downsizes the anti-resonance at 32.1 kHz and reduces positive deviations from the original transfer impedance at 15 kHz to the maximum allowed deviation of $\delta_{\max}$ as specified in Table II. The resulting transfer function is bluely highlighted in Fig. 7. The filter impedance can be deduced from the green curve.

V. Validation

Each filter stage consists of serial resistance R, inductance L and capacitance C. Since the power system electrically changes within the time of operation through switches interconnecting subnets, multiple filter stages are integrated. Fig. 8 shows a simplified schematic of a filter prototype with k stages. All stages include a MOSFET Q_k being controlled with respective gate signal. The filter circuit is connected to the power system at the terminal of system voltage V_{s}.

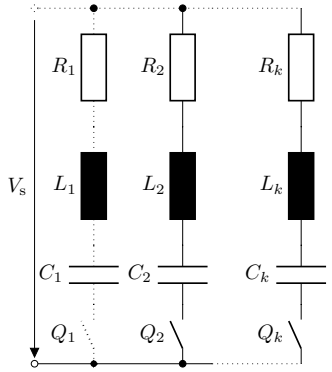

Fig. 8: Switchable bandpass filter circuit with k filter stages.

TABLE IV: Exemplary filter parameters with two stages for the reduction of anti-resonance occuring on path $i_{\mathrm{ELF}} \to u_{\mathrm{IB}}$.

1st Filter Stage		**2nd Filter Stage**	
Parameter	Value	Parameter	Value
R_1	26 mΩ	R_2	97.4 mΩ
L_1	192.7 nH	L_2	1.1 µH
C_1	134.4 µF	C_2	106.2 µF

This is the accepted version of a paper presented at 2021 IEEE 93rd Vehicular Technology Conference - VTC2021-Spring : Proceedings
http://dx.doi.org/10.1109/VTC2021-Spring51267.2021.9449066

Preferably low resistive components are integrated. For capacitances, Multilayer Ceramic (MLCC) and Aluminium Polymer structures are suitable. They show a distinct stability of capacitance up to 100 kHz. Aluminium electrolyte capacitors are less useful for this application. The parasitic inductance impacts the electrical behavior above 1 MHz and can therefore be neglected. Inductances should be of low capacitance. Würth Electronic WE-HCI components are chosen.

The MOSFET is chosen to be Infineon's IPD100N04S4-02 OptiMOS®-T2 which has a resistance of $R_{\mathrm{DS,on}} = 2\,\mathrm{m\Omega}$. The gate driver stages are set to be ordinary bipolar transistor fed gate drivers with pull-up resistor. The power system does not require high switching frequencies of the filter stages, since system states only vary in large time intervals.

The PCB is designed with a minimum impedance of 22 mΩ. The validation measurement for transfer function $i_{\mathrm{ELF}} \rightarrow u_{\mathrm{EPS}}$ at current distributor CD1 is demonstrated in Fig. 9. The damping effect at the critical frequency is lower since filter parameters deviate from the ideal calculation. Its target resistance of 14 mΩ could not practically be replicated. The filter characteristics slightly deviate due to parasitics such as the frequency-dependence of capacitance included ohmic resistances. Overall, the anti-resonance can be reduced from 743.77 mΩ to 186.58 mΩ by 75 %.

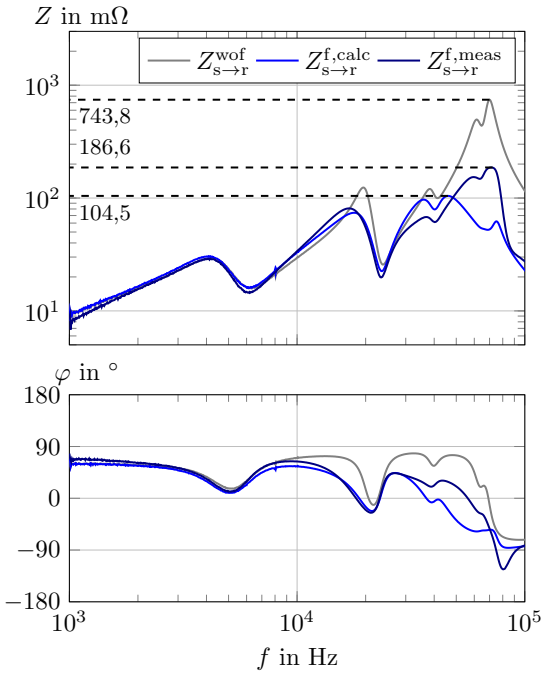

Fig. 9: Validation of filter effectiveness shows a calculated transfer function ($Z^{\mathrm{f,calc}}_{\mathrm{s\to r}}$) of path $i_{\mathrm{ELF}} \rightarrow u_{\mathrm{EPS}}$ in contrast to measured impedance ($Z^{\mathrm{f,meas}}_{\mathrm{s\to r}}$) and original ($Z^{\mathrm{wof}}_{\mathrm{s\to r}}$).

VI. Conclusion

This contribution's motivation is to investigate and improve the transient stability of automotive power systems in the frequency range of 10 kHz to 100 kHz. Transfer impedances of interest include paths from high dynamic power components such as power electronics to safety-relevant components that need to be reliably supplied. The integration of the filter stabilizes the power supply of target components. The methodology includes system identification and two-port abstraction of the extensive power system to allow resource saving computation at a downsized complexity. A developed reproducable algorithmic approach performs both filter location determination and multi-stage filter parametrization. The prototyped hardware includes four controllable filter stages. An approach to evaluate the filters location was presented.

Further investigations can be carried out on modeling with consideration of temperature and humidity. A system design to suppress disturbances of numerous paths needs to be validated. A minimum effort to suppress overall disturbances between several components needs to be examined and tested. Moreover, automating a holistic concept for the complete power system design with elevated complexity could be implemented on the basis of the established methodology.

References

[1] R. Gehring, *Beitrag zur Untersuchung und Erhöhung der Spannungsstabilität des elektrischen Energiebordnetzes im Kraftfahrzeug*. PhD thesis, Technische Universität München, 2011.

[2] J. Klötzl, *Stabilität automobiler Leistungsbordnetze*. PhD thesis, Universität der Bundeswehr München, 2012.

[3] F. Ruf, T. Kohler, M. Winter, H. Michel, J. Froeschl, C. Koelbl, B. Buchholz, and H.-G. Herzog, "Modeling of an electromechanical actuator in respect to voltage stability," in *2012 IEEE Vehicle Power and Propulsion Conference*, pp. 248–251, Oct 2012.

[4] F. Ruf, A. Barthels, G. Walla, M. Winter, T. Kohler, H. Michel, J. Froeschl, and H.-G. Herzog, "Autonomous load shutdown mechanism as a voltage stabilization method," in *2012 IEEE Vehicle Power and Propulsion Conference*, pp. 1261–1265, Oct 2012.

[5] B. Wen, D. Sarafianos, R. A. McMahon, and S. Pickering, "Understanding automotive electrical network voltage transients," in *8th IET International Conference on Power Electronics, Machines and Drives (PEMD 2016)*, pp. 1–6, April 2016.

[6] ISO Central Secretary, "Road vehicles electrical disturbances from conduction and coupling part 2: Electrical transient conduction along supply lines only," standard, ISO Central Secretary, Genf, CH, 2011.

[7] M. Baumann, C. Weissinger, and H. Herzog, "Reducing transient disturbances within automotive power systems through adapting of input circuits," in *2019 International Conference on Computing, Electronics Communications Engineering (iCCECE)*, pp. 214–218, Aug 2019.

[8] M. Baumann, C. Weissinger, and H. Herzog, "Automotive power system model validation using impulse response analysis," in *AmE 2020 - Automotive meets Electronics; 11th GMM-Symposium*, March 2020.

[9] J. C. Das, *Power System Harmonics and Passive Filter Designs*. IEEE Press, 2015.

[10] J. C. Das, "Passive filters - potentialities and limitations," *IEEE Transactions on Industry Applications*, vol. 40, no. 1, pp. 232–241, 2004.

[11] J. G. Pazmany, K. Rechberger, and B. Baeker, "Filter design in the high voltage system of electric vehicles with respect to ripple limits," in *AmE 2020 - Automotive meets Electronics; 11th GMM-Symposium*, pp. 1–6, 2020.

[12] M. Baumann, T. Brem, S. Schwimmbeck, C. Weissinger, and H. Herzog, "Impedance-based modeling of an automotive electric power steering," in *EVER 2020 - International Conference on Ecological Vehicles and Renewable Energies*, September 2020.

[13] R. R. Singh, *Network Analysis and Synthesis*. Mc Graw Hill India, 1 ed., 2013.

[14] O. Wing, *Classical Circuit Theory*. Springer Science+Business Media, LLC, 2008.

[15] B. Gustavsen and A. Semlyen, "Rational approximation of frequency domain responses by vector fitting," *IEEE Transactions on Power Delivery*, vol. 14, no. 3, pp. 1052–1061, 1999.

[16] B. Gustavsen, "Improving the pole relocating properties of vector fitting," *IEEE Transactions on Power Delivery*, vol. 21, no. 3, pp. 1587–1592, 2006.

This is the accepted version of a paper presented at 2021 IEEE 93rd Vehicular Technology Conference - VTC2021-Spring : Proceedings
http://dx.doi.org/10.1109/VTC2021-Spring51267.2021.9449066